

Magnetic field effects in the near-field radiative heat transfer between planar structures

E. Moncada-Villa¹ and J. C. Cuevas²

¹*Escuela de Física, Universidad Pedagógica y Tecnológica de Colombia,
Avenida Central del Norte 39-115, Tunja, Colombia and*

²*Departamento de Física Teórica de la Materia Condensada and Condensed Matter Physics Center (IFIMAC),
Universidad Autónoma de Madrid, E-28049 Madrid, Spain*

(Dated: December 11, 2021)

One of the main challenges in the field of thermal radiation is to actively control the near-field radiative heat transfer (NFRHT) between closely spaced bodies. In this context, the use of an external magnetic field has emerged as a very attractive possibility and a plethora of physical phenomena have been put forward in the last few years. Here, we predict some additional magnetic-field-induced phenomena that can take place in the context of NFRHT between planar layered structures containing magneto-optical (MO) materials (mainly doped semiconductors like InSb). In particular, we predict the possibility of increasing the NFRHT upon applying an external magnetic field in an asymmetric structure consisting of two infinite plates made of InSb and Au. We also study the impact of a magnetic field in the NFRHT between structures containing MO thin films and show that the effect is more drastic than in their bulk counterparts. Finally, we systematically investigate the anisotropic thermal magnetoresistance, i.e., the dependence of the radiative heat conductance on the orientation of an external magnetic field, in the case of two infinite plates made of InSb and show that one can strongly modulate the NFRHT by simply changing the orientation of the magnetic field. All the phenomena predicted in this work can be experimentally tested with existent technology and provide a new insight into the topic of active control of NFRHT.

I. INTRODUCTION

The field of thermal radiation has been revolutionized in recent years by the confirmation of the prediction that the radiative heat transfer between closely spaced objects can largely overcome the Planckian or black-body limit, for recent reviews see Refs. [1, 2]. Traditionally, our understanding of thermal radiation has been based on Planck's law and the concept of a black body. This law establishes, in particular, an upper limit for the amount of heat that two bodies can exchange via electromagnetic radiation (Stefan-Boltzmann's law). However, Planck's law, which is based on ray optics, has obvious limitations and, in particular, fails to describe the radiative heat transfer between two objects when they are separated by distances below the thermal wavelength λ_{Th} ($\sim 10 \mu\text{m}$ at room temperature). This was first recognized in the early 1970s by Polder and van Hove [3], who made use of the theoretical framework of fluctuational electrodynamics derived in the 1950s by Rytov [4, 5] to predict that the radiative heat transfer between two infinite parallel plates could greatly overcome the black-body limit by bringing them sufficiently close (that is, below λ_{Th}). They showed that in this near-field regime the radiative heat transfer can be entirely dominated by evanescent waves, which give an extra contribution that is not taken into account in Stefan-Boltzmann's law. The NFRHT enhancement was already hinted in several experiments in the late 1960's [6, 7], but due to experimental challenges it took more than 30 years to confirm it unambiguously. In the last decade or so, different experiments have demonstrated the possibility to overcome the black-body limit in the near-field regime by exploring a large

variety of materials and body shapes [8–32]. Moreover, these experiments have confirmed the validity of the theory of fluctuational electrodynamics and they have also triggered off the hope that NFRHT may have an impact in different thermal technologies, see Refs. [1, 2].

Now that, to a large extent, the basic principles governing NFRHT have been established, one of the central challenges is to learn how to actively control thermal emission in the near-field regime, something that would be essential for its use in a variety of applications. In this context, the possibility of using an external magnetic field, mimicking somehow what is being done in spintronics, has emerged as one of the most interesting ideas. The use of an external magnetic field to control the NFRHT between magneto-optical (MO) materials was first put forward in our work of Ref. [33]. There, we showed that the NFRHT between two parallel plates made of doped semiconductors can be strongly affected by the application of a static magnetic field and relative changes of up to 700% can be induced with fields of a few Teslas [33]. Ever since, a plethora of thermomagnetic effects have been predicted. Thus, for instance, it has been suggested that the lack of reciprocity in MO systems can lead to novel phenomena such as a near-field thermal Hall effect [34] or the existence of a persistent heat current [35]. It has also been shown that MO materials under a static magnetic field can exhibit the near-field thermal analogues of the key effects in the field of spintronics such as a giant thermal magnetoresistance [36] or an anisotropic thermal magnetoresistance [37]. Some of these phenomena and other ones have been reviewed in Ref. [38].

Although the fundamental importance of the ther-

momagnetic effects mentioned above is unquestionable, many of them deal with submicron particles and many-body systems, which are very challenging to explore experimentally. Fortunately, there are still many interesting open questions related to the magnetic field dependence of the NFRHT between planar structures containing MO materials. Thus, for instance, in our work of Ref. [33] on the NFRHT between infinite plates made of doped semiconductors, an ideal class of MO materials, we always found that the magnetic field reduces the radiative heat conductance, irrespective of its magnitude and direction. Thus, a natural question arises on whether it is possible to enhance the NFRHT upon applying an external magnetic field. Another interesting question is related to the magnetic field dependence of the NFRHT between structures containing thin films of MO materials. As we discovered in the case of doped semiconductors, the application of a magnetic field in these materials leads to the appearance of hyperbolic modes [33, 39], very much like in hyperbolic metamaterials where the diagonal components of the permittivity tensor have different signs [40]. These hyperbolic modes were shown to play a very important role in the field-dependent NFRHT between doped semiconductors [33], and since they are propagating waves, they are expected to be very sensitive to the presence of substrates in structures containing thin films. So, in this respect, one wonders what is the magnetic field dependence of the NFRHT in thin-film structures of MO materials. On the other hand, it has been recently shown in the context of submicron MO particles that the NFRHT is very sensitive to the orientation of the magnetic field with respect to the transport direction [37]. The variation of the radiative heat conductance with the orientation of the external field gives rise to thermal analog of the anisotropic magnetoresistance (AMR) in spintronics and it has been referred to as anisotropic thermal magnetoresistance (ATMR) [37]. In that work, the field modulation of the NFRHT in submicron InSb particles was found to be orders of magnitude larger than in the corresponding electrical conductance in AMR devices. Moreover, the ATMR phenomenon was suggested to have potential applications in the field of ultrafast thermal management as well as magnetic and thermal remote sensing. Given the fundamental interest in this phenomenon, it would be highly desirable to analyze it in the context of macroscopic planar structures, where it would be much easier to investigate experimentally. The goal of this work is to tackle all these open questions from the theoretical point of view and to provide very concrete predictions that could potentially be tested with existent experimental techniques.

The rest of the paper is organized as follows. Section II introduces the systems under study and presents the general formalism that we use for the description of NFRHT in the presence of a magnetic field. In Sec. III we study the NFRHT between two parallel plates made of InSb and, and we show that it is possible to enhance it by applying an external magnetic field. Section IV is devoted

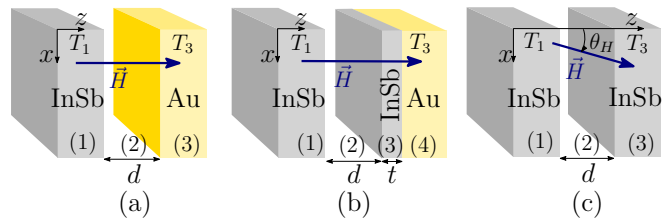


FIG. 1. Schematic representation of the systems under study. (a) Two semi-infinite plates made of n -doped InSb and Au at temperatures T_1 and T_3 , respectively, separated by vacuum gap of size d and subjected to an external magnetic field that is perpendicular to the plates. (b) A semi-infinite plate of n -doped InSb at temperature T_1 separated by a vacuum gap (of size d) from a InSb thin film of thickness t , deposited on an Au semi-infinite substrate. The thin film and the substrate have the same temperature T_3 . (c) Two semi-infinite plates made of n -doped InSb at temperatures T_1 and T_3 , respectively, separated by vacuum gap of size d and subjected to an external magnetic field in the xz that forms an angle θ_H with the z -direction. In all three cases the vacuum gap is referred to as medium 2.

to the analysis of the magnetic field dependence of the NFRHT between structures containing thin films of MO materials. Section V presents a detailed discussion of the anisotropic thermal magnetoresistance in a system comprising two infinite parallel plates made of InSb. Finally, Sec. VI summarizes the main conclusions of our work.

II. SYSTEMS UNDER STUDY AND THEORETICAL APPROACH

Our main goal is to compute the radiative heat transfer between different layered systems in the presence of an external dc magnetic field, see Fig. 1, within the framework of fluctuational electrodynamics [4, 5]. All the systems considered here consist of two layered systems separated by a vacuum gap (medium 2) of size d and subjected to an external magnetic field, \vec{H} , that can point in any direction. In general, the layer materials can have MO activity, i.e., under the presence of a magnetic field these materials are optically anisotropic materials and their permittivity can be described by a tensor of the form [41]

$$\hat{\epsilon} = \begin{pmatrix} \epsilon_{xx} & \epsilon_{xy} & \epsilon_{xz} \\ \epsilon_{yx} & \epsilon_{yy} & \epsilon_{yz} \\ \epsilon_{zx} & \epsilon_{zy} & \epsilon_{zz} \end{pmatrix}. \quad (1)$$

Here, as we indicate in Fig. 1, x and y lie in the planes of the layer interfaces and z corresponds to the surface normal. The components of this permittivity tensor depend, in general, on the applied magnetic field, as we shall specify below, and on the frequency (local approximation). Let us remind that the off-diagonal elements in Eq. (1) are responsible for the polarization conversion and all the typical MO effects (Faraday effect, Kerr effects, etc.)

[41]. Thus, our problem is to compute the radiative heat transfer between two anisotropic planar layered systems. This generic problem has been addressed before in the literature [33, 42] and we just recall here the central result. The net power per unit of area exchanged between two anisotropic layered systems is given by the following Landauer-like expression [33, 42]

$$Q = \int_0^\infty \frac{d\omega}{2\pi} [\Theta_1(\omega) - \Theta_3(\omega)] \int \frac{d\mathbf{k}}{(2\pi)^2} \tau(\omega, \mathbf{k}, d), \quad (2)$$

where $\Theta_i(\omega) = \hbar\omega/[\exp(\hbar\omega/k_B T_i) - 1]$, T_i is the absolute temperature of the layer i , ω is the radiation frequency, $\mathbf{k} = (k_x, k_y)$ is the wave vector parallel to the surface planes, and $\tau(\omega, \mathbf{k}, d)$ is the total transmission probability of the electromagnetic propagating waves ($|\mathbf{k}| = k < \omega/c$), as well as evanescent ones ($k > \omega/c$). This transmission coefficient is expressed as [33, 42]

$$\tau(\omega, \mathbf{k}, d) = \begin{cases} \text{Tr} \left\{ [\hat{1} - \hat{\mathcal{R}}_{21} \hat{\mathcal{R}}_{21}^\dagger] \hat{\mathcal{D}}^\dagger [\hat{1} - \hat{\mathcal{R}}_{23}^\dagger \hat{\mathcal{R}}_{23}] \hat{\mathcal{D}} \right\}, & k < \omega/c \\ \text{Tr} \left\{ [\hat{\mathcal{R}}_{21} - \hat{\mathcal{R}}_{21}^\dagger] \hat{\mathcal{D}}^\dagger [\hat{\mathcal{R}}_{23}^\dagger - \hat{\mathcal{R}}_{23}] \hat{\mathcal{D}} \right\} e^{-2|q_2|d}, & k > \omega/c \end{cases}, \quad (3)$$

where $q_2 = \sqrt{\omega^2/c^2 - k^2}$ is the z -component of the wave vector in the vacuum gap, c is the velocity of light in vacuum and $\hat{\mathcal{D}} = [\hat{1} - \hat{\mathcal{R}}_{21} \hat{\mathcal{R}}_{23} e^{2iq_2 d}]^{-1}$ describes the usual Fabry-Pérot-like denominator resulting from the multiple scattering between the two interfaces. The 2×2 matrices $\hat{\mathcal{R}}_{ij}$ are the reflections matrices characterizing the two

interfaces at both sides of the gap. These matrices have the following generic structure

$$\hat{\mathcal{R}}_{ij} = \begin{pmatrix} r_{ij}^{s,s} & r_{ij}^{s,p} \\ r_{ij}^{p,s} & r_{ij}^{p,p} \end{pmatrix}, \quad (4)$$

where $r_{ij}^{\alpha,\beta}$ with $\alpha, \beta = s, p$ (or TE, TM) is the reflection amplitude for the scattering of an incoming α -polarized plane wave into an outgoing β -polarized wave. In practice, we compute numerically the different reflection matrices appearing in Eq. (3) by using the scattering-matrix approach for anisotropic multilayer systems that is described in Refs. [33, 43].

Throughout this work we focus on the analysis of the radiative linear heat conductance per unit of area, h , which is known as the heat transfer coefficient. This coefficient is given by

$$h(T, d) = \lim_{\Delta T \rightarrow 0^+} \frac{Q(T_1 = T + \Delta T, T_3 = T, d)}{\Delta T}. \quad (5)$$

Additionally, we define the spectral heat flux, h_ω , as the heat transfer coefficient per unit of frequency. Moreover, in all the calculations reported in this work we shall assume room temperature ($T = 300$ K).

In the following sections we shall apply the general formalism above to the systems depicted in Fig. 1. All these systems contain at least one layer made of n -doped InSb under the action of a magnetic field in the xz plane and forming an angle θ_H with the z -axis. As a consequence, the InSb can exhibit an optical anisotropy that can be described by the following permittivity tensor [44]

$$\hat{\epsilon} = \begin{pmatrix} \epsilon_1 \cos^2 \theta_H + \epsilon_3 \sin^2 \theta_H & -i\epsilon_2 \cos \theta_H & \frac{1}{2}(\epsilon_1 - \epsilon_3) \sin 2\theta_H \\ i\epsilon_2 \cos \theta_H & \epsilon_1 & i\epsilon_2 \sin \theta_H \\ \frac{1}{2}(\epsilon_1 - \epsilon_3) \sin 2\theta_H & -i\epsilon_2 \sin \theta_H & \epsilon_1 \sin^2 \theta_H + \epsilon_3 \cos^2 \theta_H \end{pmatrix}, \quad (6)$$

with

$$\begin{aligned} \epsilon_1(H) &= \epsilon_\infty \left(1 + \frac{\omega_L^2 - \omega_T^2}{\omega_T^2 - \omega^2 - i\Gamma\omega} + \frac{\omega_p^2(\omega + i\gamma)}{\omega[\omega_c^2 - (\omega + i\gamma)^2]} \right), \\ \epsilon_2(H) &= \frac{\epsilon_\infty \omega_p^2 \omega_c}{\omega[(\omega + i\gamma)^2 - \omega_c^2]}, \\ \epsilon_3 &= \epsilon_\infty \left(1 + \frac{\omega_L^2 - \omega_T^2}{\omega_T^2 - \omega^2 - i\Gamma\omega} - \frac{\omega_p^2}{\omega(\omega + i\gamma)} \right). \end{aligned} \quad (7)$$

Here, ϵ_∞ is the high-frequency dielectric constant, ω_L (ω_T) is the longitudinal (transverse) optical phonon frequency, $\omega_p^2 = ne^2/(m^* \epsilon_0 \epsilon_\infty)$ is the plasma frequency of free carriers of density n and effective mass m^* , Γ (γ) is the phonon (free-carrier) damping constant, and $\omega_c = eH/m^*$ is the cyclotron frequency, which depends on the intensity of the applied magnetic field. For the sake of concreteness, we shall assume throughout this

work that $\epsilon_\infty = 15.7$, $\omega_L = 3.62 \times 10^{13}$ rad/s, $\omega_T = 3.39 \times 10^{13}$ rad/s, $\Gamma = 5.65 \times 10^{11}$ rad/s, $\gamma = 3.39 \times 10^{12}$ rad/s, $n = 1.07 \times 10^{17}$ cm $^{-3}$, $m^*/m = 0.022$, and $\omega_p = 3.14 \times 10^{13}$ rad/s [44]. As a reference for our discussions below, we show in Fig. 2 the real and the imaginary part of the function $\epsilon_1(H)$ for different values of the magnetic field in the frequency range of relevance for the radiative heat transfer problems studied in this work. At zero field, InSb is an optically isotropic material and ϵ_1 is its dielectric function. In this case, one can distinguish three frequency regions. First, for frequencies around ω_T , the frequency of the transversal phonon, $\epsilon_1(H = 0)$ exhibits the typical Lorentz-like behavior associated to an optical phonon with a sign change in the real part and a peak in the imaginary part. In the region below ω_T , $\epsilon_1(H = 0)$ follows the typical Drude-like behavior of a metal, and above ω_T it behaves as a non-lossy dielectric. At a finite magnetic field, the real part of $\epsilon_1(H)$ ex-

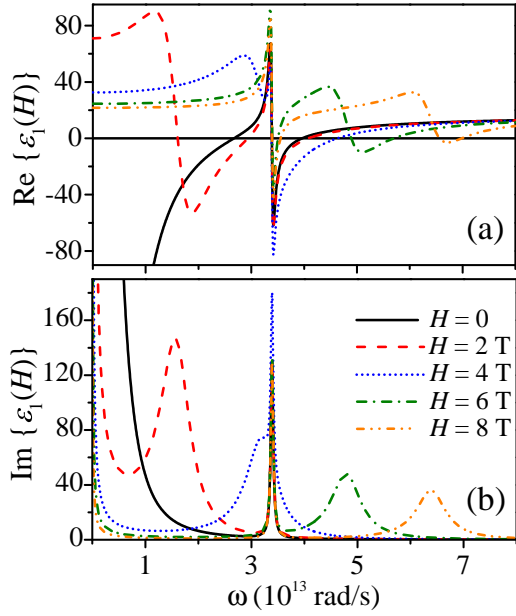


FIG. 2. (a) Real and (b) imaginary parts of the dielectric function $\epsilon_1(H)$, see Eq. (7), as a function of the frequency for different values of the magnitude of the external magnetic field. We remind that $\epsilon_1(H = 0) = \epsilon_3$.

hibits additional sign changes, in particular, around the cyclotron frequency which is equal to $\omega_c = 8.02 \times 10^{12}$ rad/s for a field of 1 T. Notice also the appearance of the corresponding peak in the imaginary part at ω_c . Let us also recall that $\epsilon_3 = \epsilon_1(H = 0)$. Thus, one can see that there are regions at finite external field in which the real parts of ϵ_1 and ϵ_3 , which mainly determine the diagonal components of the permittivity tensor, have opposite signs. This fact implies the appearance of hyperbolic modes, as it has been discussed before [33, 39].

On the other hand, we shall also consider layers made of Au. For this metal, we shall use the following Drude-like relative permittivity [45]

$$\epsilon_{\text{Au}} = \epsilon_{\infty, \text{Au}} - \frac{\omega_{p, \text{Au}}^2}{\omega(\omega + i\gamma_{\text{Au}})}, \quad (8)$$

where $\epsilon_{\infty, \text{Au}} = 1$, $\omega_{p, \text{Au}} = 1.71 \times 10^{16}$ rad/s and $\gamma_{\text{Au}} = 1.22 \times 10^{14}$ rad/s. We remark that we shall ignore the effect of the magnetic field in the gold permittivity, which is justified by the huge plasma frequency as compared to the cyclotron frequency for realistic values of the magnetic field.

III. MAGNETIC FIELD INDUCED ENHANCEMENT OF THE NFRHT

In previous studies of the radiative heat transfer between two MO objects, it has always been found that the application of an external magnetic field reduces the linear heat conductance, irrespective of the orientation of

the field. For instance, we showed in Ref. [33] that this was the case in parallel plates made of identical materials (doped InSb and doped Si), for both the near-field and the far-field regime. Something similar was found in Ref. [37] in the case of two identical spherical particles made of InSb of arbitrary size. However, there is no fundamental reason why the magnetic field should always reduce the radiative heat transfer between two bodies and the goal of this section is to show that indeed an external field can enhance, in particular, the NFRHT between two objects. For this purpose, we analyze in this section the asymmetric system of Fig. 1(a) which consists of two infinite parallel plates made of doped InSb (a MO material) and Au. For the sake of concreteness, we shall assume that the external magnetic field is applied perpendicularly to the plates. In this particular case, the magnetic-field-dependent permittivity tensor of InSb adopts the form

$$\hat{\epsilon} = \begin{pmatrix} \epsilon_1(H) & -i\epsilon_2(H) & 0 \\ i\epsilon_2(H) & \epsilon_1(H) & 0 \\ 0 & 0 & \epsilon_3 \end{pmatrix}, \quad (9)$$

where the different elements are given by Eq. (7) and the diagonal components are shown in Fig. 2 for different values of the magnetic field.

In Fig. 3(a) we summarize the results for the heat transfer coefficient as a function of the separation between the InSb and the Au plates for different values of the external magnetic field, which is applied perpendicularly to the plates. The first thing to notice is that, as expected, the heat transfer coefficient is clearly lower than for the symmetric cases InSb-InSb [33] and Au-Au [45], irrespective of the gap size. This is simply due to the mismatch between the dielectric functions of both materials. Actually, the heat conductance only overcomes the black-body limit ($6.124 \text{ W m}^{-2} \text{ K}^{-1}$) for very small gap below 10 nm. More importantly, the magnetic field enhances the conductance in practically all the near-field regime (apart from very small gaps below 10 nm). This can be clearly seen in Fig. 3(b) where we show the ratio between the heat transfer coefficient with and without magnetic field. Notice that the conductance is enhanced by more than 20% for fields of 6-8 T for gaps between 10 and 100 nm. Notice also that in the far-field regime (beyond $10 \mu\text{m}$), the magnetic field barely changes the radiative heat conductance.

What is the physical origin for this magnetic-field-induced enhancement of the NFRHT? Let us recall that in the symmetric case InSb-InSb it was found that the field reduces the NFRHT because the p -polarized (TM) surface modes that dominate the heat transfer in the near-field regime at zero field are progressively replaced by hyperbolic modes, which turn out to be less efficient transferring the heat across the gap [33]. In this case, the situation is clearly different. First, the gap dependence that one can see in Fig. 3(a) in the range 10-1000 nm, where the conductance enhancement is most notable, suggests that the NFRHT is not dominated by surface

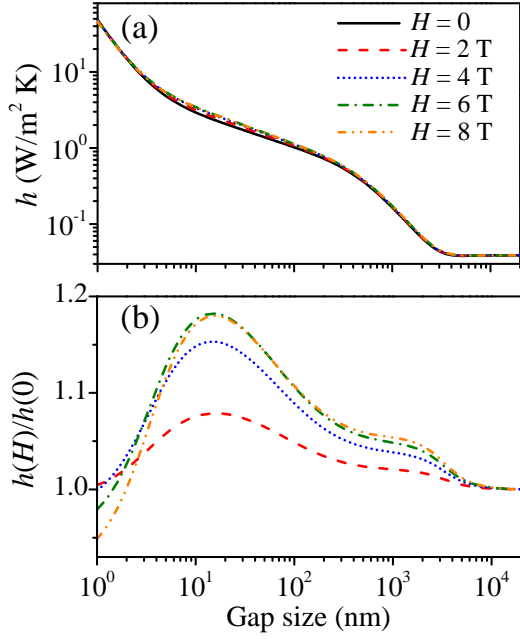


FIG. 3. (a) Heat transfer coefficient for the system of Fig. 1(a) as a function of the gap size for different values of the magnetic field perpendicular to the plate surfaces. (b) The corresponding ratio between the heat transfer coefficient at a given value of the field magnitude and the zero-field coefficient as a function of the gap size.

modes, but rather by frustrated total internal reflection modes, like in the Au-Au case [45]. These modes are evanescent in the vacuum gap, but they are propagating inside the materials. Moreover, in this case, and because of the off-diagonal elements in the permittivity tensor of Eq. (9), there is polarization conversion, whose role is not clear a priori and impedes to properly define the separate contributions of TE and TM modes. For these reasons, and in order to shed light on the physical interpretation, we have tested the validity of an approximation where we ignore the role of polarization conversion by setting the off-diagonal reflection coefficients to zero, i.e., we set $r_{ij}^{s,p} = r_{ij}^{p,s} = 0$ in Eq. (4). We stress that this is different from assuming that the off-diagonal elements of the InSb permittivity tensor vanish. Actually, those elements play a non-negligible role in the diagonal reflection coefficients ($r_{ij}^{s,s}$ and $r_{ij}^{p,p}$). As we show in Fig. 4(a) for two different values of the magnetic field, the approximation neglecting polarization conversion accurately reproduces the exact results. This fact allows us to conclude that the field-induced enhancement is not due to the polarization conversion, but rather to a modification of the probability of the evanescent waves. In particular, in the range where the near-field conductance is enhanced by the field, such an enhancement turns out to be mainly due to the enhanced probability of the TE modes, as we now proceed to show.

To illustrate that the TE modes are responsible for the field-induced enhancement, we first analyze the spectral

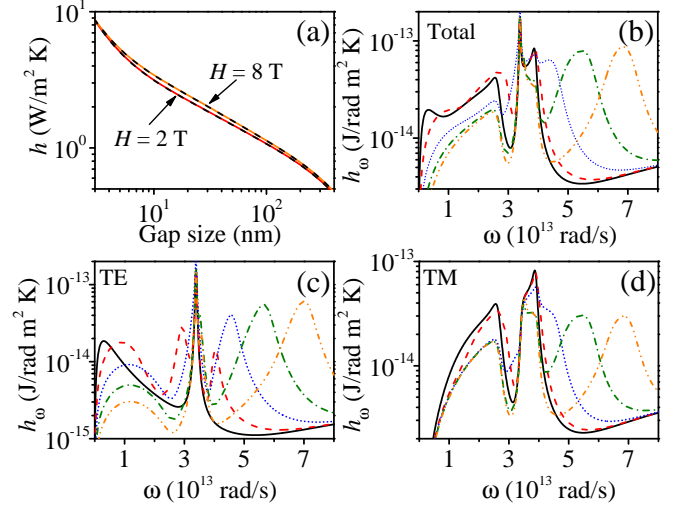


FIG. 4. (a) Heat transfer coefficient as a function of the gap size for the system of Fig. 1(a) for a perpendicular magnetic field with magnitude of 2 and 8 T. The solid lines correspond to the exact results and the dashed lines to the results obtained by considering no polarization conversion, that is, with $r_{ij}^{s,p} = r_{ij}^{p,s} = 0$ in Eq. (4). (b) The corresponding spectral heat flux computed with the exact formalism as a function of the frequency for a gap $d = 10$ nm and different values of the magnitude of the external (perpendicular) field. The magnetic field values corresponding to the different lines are those indicated in the legend of Fig. 3(a). In panels (c) and (d), we present, within the approximation $r_{ij}^{s,p} = r_{ij}^{p,s} = 0$, the spectral heat flux as a function of frequency for TE (s -polarized) and TM (p -polarized) waves, respectively, for a gap $d = 10$ nm and different values of the magnitude of the external (perpendicular) field.

heat flux. The total contribution to this quantity calculated with the exact formalism for a gap $d = 10$ nm is shown in Fig. 4(b) as a function of the frequency and for different values of the magnetic field. The corresponding contributions from TE and TM modes calculated within the approximation $r_{ij}^{s,p} = r_{ij}^{p,s} = 0$ are shown in panels (c) and (d) of that figure, respectively. Although both contributions change with the applied field, the enhancement is clearly due to the TE modes. For this polarization (TE), the zero-field spectral heat flux is dominated by a peak at the frequency of the optical phonon $\omega_T = 3.39 \times 10^{13} \text{ rad/s}$. As the field increases, there appear additional peaks in the spectral function at positions that are intimately related to the frequencies at which the real part of $\epsilon_1(H)$ changes sign. In particular, notice the presence of a peak that follows closely, but not exactly, cyclotron frequency, which proportional to the field and is equal to $8.02 \times 10^{12} \text{ rad/s}$ for a field of 1 T. For the TM polarization, the main contributions at zero field to the spectral heat flux come from the Reststrahlen band (between ω_T and ω_L) due to surface phonon polaritons in InSb and at low frequencies due to surface plasmon polaritons in InSb. At finite fields, there are additional contributions coming mainly from frequencies around the cyclotron fre-

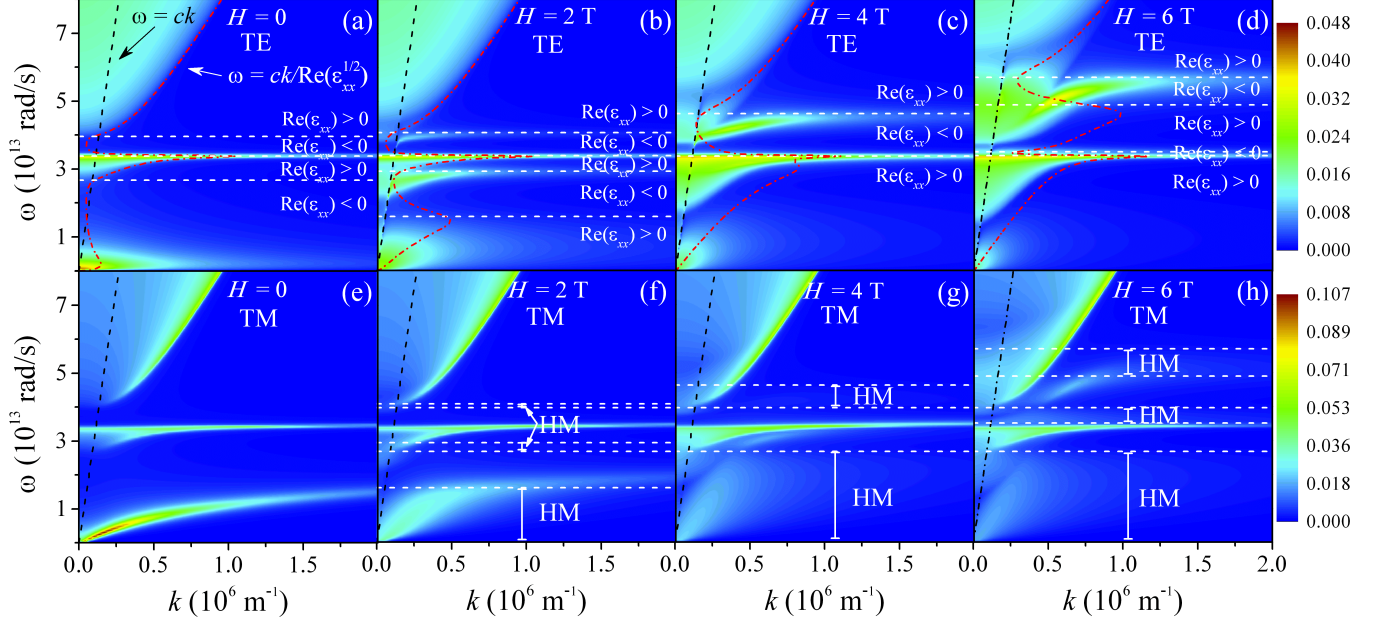


FIG. 5. Transmission coefficient for *s*-polarized (TE) [panels (a-d)] and *p*-polarized (TM) [panels (e-h)] waves, as a function of the magnitude of the parallel wave vector and frequency for the system of Fig. 1(a) with a gap size $d = 10$ nm. These transmissions were computed with the approximation neglecting polarization conversion and the different panels correspond to different values the external (perpendicular) field. The black dashed lines correspond to the light line in vacuum, $\omega = ck$, while the red dashed-dotted lines in panels (a-d) correspond to the light line inside InSb, $\omega = ck\text{Re}(\epsilon_{xx}^{1/2})$. The horizontal dashed lines delimit the different regions where hyperbolic modes (HM) exist for the TM polarization and in the upper panels we specify the sign of $\text{Re}\{\epsilon_1(H)\}$ in these different regions.

quency.

To further clarify the nature of the relevant electromagnetic modes we analyze their corresponding transmission coefficients (ignoring polarization conversion). These coefficients are shown in Fig. 5 as a function of the frequency and the magnitude of the parallel wave vector for a gap of 10 nm. Focusing on the transmission of the TE modes (upper panels), we see that at zero field the main contributions come from modes that are evanescent in the vacuum gap, but they are propagating inside the InSb plate (notice that they lie on the left of the light line inside InSb). In other words, these are frustrated total internal reflection modes. At finite magnetic field, the real part of $\epsilon_{xx} = \epsilon_1$ exhibits additional sign changes and, in particular, there are several regions where the real parts of ϵ_{xx} and $\epsilon_{zz} = \epsilon_3$ have opposite signs, see Fig. 2. This latter fact means that the InSb can exhibit hyperbolic modes in those frequency regions for TM polarization, as it was amply discussed in Ref. [33]. These regions with hyperbolic modes are denoted by HM in the lower panels of Fig. 5. However, the dispersion relation of the ordinary waves for TE polarization is solely determined by $\epsilon_{xx} = \epsilon_1(H)$ and the new peaks in the spectral heat flux for this polarization, see Fig. 4(c), appear at frequencies at which the real part of ϵ_{xx} vanishes, while its imaginary part remains relatively appreciable. As one can see in the upper panels of Fig. 5, the main change

induced by the external field around those frequencies is the enhanced contribution of evanescent waves with larger values of the parallel wave vector, which naturally increases the total contribution to the heat transfer. The enhancement of the contribution of these modes is due to reduction of the impedance mismatch between InSb and the vacuum gap, which in turn is due to the vanishing value of ϵ_{xx} . This reduction of the impedance mismatch is also signaled by the fact that around those frequencies the light lines inside InSb and in vacuum tend to approach each other, see upper panels of Fig. 5. With respect to the TM modes, see Fig. 5(e-h), they are less sensitive to the external magnetic field and, in spite of the appearance of hyperbolic modes, their contribution to the heat transfer continues to be dominated by frequencies inside the Reststrahlen band.

So, in short, we have seen in this section that an external magnetic field can indeed enhance the NFRHT in an asymmetric situation comprising an InSb and an Au plate. We have traced back the conductance enhancement in the near-field regime to an increase in the contribution of the evanescent TE waves that overcomes the deleterious effect of the magnetic field on the evanescent TM waves due to the appearance of hyperbolic modes.

IV. MAGNETIC FIELD DEPENDENCE OF THE RADIATIVE HEAT TRANSFER IN THIN FILMS

Recently, it has been experimentally demonstrated that thin films made of polar dielectrics may support NFRHT enhancements comparable to those of bulk samples when the gap size is smaller than the film thickness [22]. This is possible due to the fact that in these materials the NFRHT is dominated by the contribution of surface phonon polaritons (SPhPs) whose penetration depth is comparable to the gap size. In the case of doped semiconductors, like InSb, the NFRHT is also dominated by surface electromagnetic modes due to either SPhPs or surface plasmon polaritons (SPPs). Therefore, similar NFRHT enhancements are also expected in thin films made of these materials. Moreover, since the application of a magnetic field in doped semiconductors results in the generation of hyperbolic modes, which have propagating character even in the near-field regime and therefore propagate further inside the materials, one could expect more drastic magnetic-field effects in thin-film structures of doped semiconductors than in their bulk counterparts. Motivated by this idea, we study in this section the magnetic-field dependence of the radiative heat transfer between structures containing thin films of MO materials. In particular, we investigate the system of Fig. 1(b), which consists of an InSb plate and an InSb thin film of thickness t deposited on a semi-infinite Au layer. For the sake of concreteness, we shall assume that the external field is applied perpendicularly to the plates, see Fig. 1(b). Thus, as in the previous section, the magnetic-field-dependent permittivity tensor of InSb is given by Eq. (9).

Let us start by analyzing the system of Fig. 1(b) in the absence of an external magnetic field. In Fig. 6(a) we present the results for the heat transfer coefficient as a function of the gap size for a variable thickness of the InSb layer deposited on Au ranging from 5 nm to a bulk sample. As one can see, in the near-field regime (mainly below $1\ \mu\text{m}$), when the gap size is smaller than the InSb layer thickness, the value of the heat transfer coefficient is the same, irrespective of layer thickness. This is exactly the same behavior that takes place in the case of polar dielectrics (like SiO_2 , SiN , etc.) [22, 46–48] and it has the same physical origin. This behavior is due to the fact that the NFRHT is dominated by cavity surface modes, in this case SPPs and SPhPs [33], whose penetration depth scales with the gap size and, therefore, they become more confined as the gap is reduced. This explains the thickness independence of the NFRHT when the gap is sufficiently small (smaller than the layer thickness).

We turn now to discuss how the presence of an external magnetic field alters the NFRHT in these multilayer structures. In Fig 6(b) we present the results for the ratio $h(0)/h(H)$ of the heat transfer coefficient without and with a field applied as a function of the gap size for different values of a perpendicular magnetic field. In particular, we present results for three different values

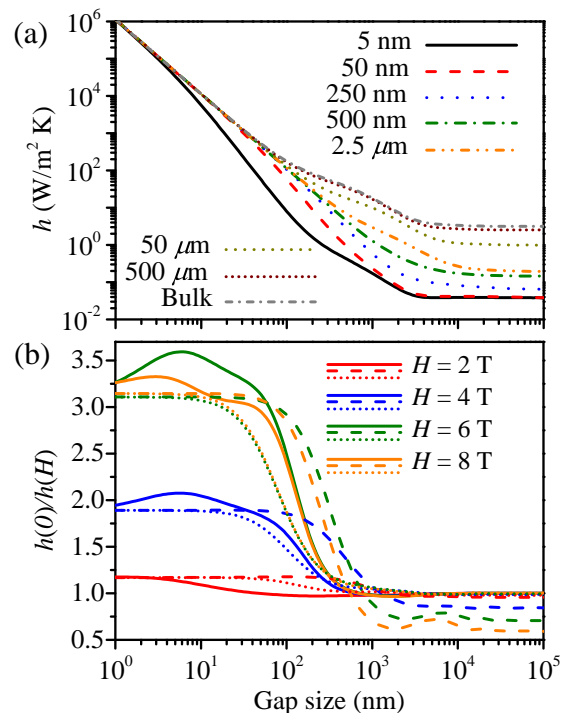


FIG. 6. (a) Heat transfer coefficient as a function of the gap size for the system of Fig. 1(b) in the absence of an external magnetic field. The different curves correspond to different values of the InSb layer thickness, t . (b) Ratio of the zero-field heat transfer coefficient and the heat transfer coefficient at a given magnetic field for the system of Fig. 1(b) as a function of the gap size. The different curves correspond to different values of the magnitude of the field and to different values of the InSb film thickness: 5 nm (solid lines), $2.5\ \mu\text{m}$ (dashed lines), and $500\ \mu\text{m}$ (dotted lines).

of the InSb layer thickness: $t = 5\ \text{nm}$, a very thin film, $t = 2.5\ \mu\text{m}$, an intermediate thickness, and $t = 500\ \mu\text{m}$, which basically corresponds to a bulk layer. The first thing to notice is that in most cases, irrespective of the gap size, InSb layer thickness, and magnitude of the field, the radiative heat conductance tends to be decreased by the field, as compared to the zero-field case. This is, in particular, what occurs both in the very thin and in the bulk case (this latter situation was extensively analyzed in Ref. [33]) both in the near- and in the far-field regime. Let us recall that this field-induced reduction is mainly due to the appearance of hyperbolic modes in certain frequency regions, modes that are less effective transferring the heat across the gap than the surface modes that dominate the NFRHT in the absence of field. Concerning the thickness dependence of the heat transfer coefficient, there are two salient effects. First, the largest field-induced reductions of the NFRHT occur for the thinnest case. This is expected since the hyperbolic modes that appear at finite field have long penetration depths (much longer than surface modes) and, therefore, are more sensitive to the presence of the Au substrate.

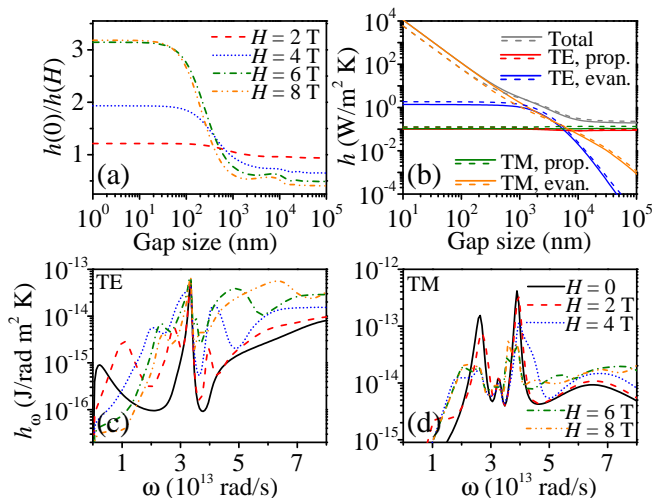


FIG. 7. (a) Ratio of the zero-field heat transfer coefficient and the heat transfer coefficient for the system of Fig. 1(b) as a function of the gap size and for InSb layer thickness $t = 2.5 \mu\text{m}$. The different curves correspond to different values of the magnitude of the field and the results were computed with the diagonal approximation: $r_{ij}^{s,p} = r_{ij}^{p,s} = 0$ in Eq. (4). Notice that these results accurately reproduce the exact results shown in Fig 6(b). (b) The corresponding heat transfer coefficient computed with the diagonal approximation as a function of the gap size for two values of the magnetic field: $H = 0$ T (solid lines) and $H = 4$ T (dashed lines). We show the total contribution to the heat transfer coefficient as well as the different individual contributions from TE and TM modes, both propagating and evanescent. Panels (c) and (d) show the spectral heat flux calculated with the diagonal approximation as a function of frequency for TE (s -polarized) and TM (p -polarized) waves, respectively, for a gap $d = 1 \mu\text{m}$ and different values of the magnitude of the external (perpendicular) field.

In practice, this means that the substrate reduces the probability of the hyperbolic modes and, in turn, their contribution to the heat transfer. The second interesting effect is the fact that in the case of intermediate thickness values, see curves for $t = 2.5 \mu\text{m}$, there is a gap range (between 1 and $10 \mu\text{m}$) where the NFRHT is actually enhanced by the field (i.e., the ratio $h(0)/h(H)$ is smaller than 1), and this enhancement persists in the far-field regime. This behavior is at variance with the bulk case and we shall try to explain its physical origin in what follows, focusing on the near-field regime.

The first step to understand this field-induced enhancement is to examine the validity of the diagonal approximation discussed in the previous section where the polarization conversion is ignored by setting $r_{ij}^{s,p} = r_{ij}^{p,s} = 0$ in Eq. (4). As we show in Fig. 7(a), this approximation accurately reproduces the exact results shown in Fig 6(b) for the field dependence of the heat transfer coefficient for a thickness $t = 2.5 \mu\text{m}$. Thus, we shall use this approximation to shed light on the origin of the field-induced enhancement. Within this diagonal approxima-

tion we can unambiguously define the contribution of TE and TM modes, both propagating and evanescent. We show all those contributions in Fig. 7(b) as a function of the gap size for $t = 2.5 \mu\text{m}$ and two values of the field: 0 and 4 T. From these results we can learn two basic things. First, the field-induced enhancement of the NFRHT occurs in a gap region in which the contributions of evanescent TM and TE modes are comparable, i.e., for separations where surface modes do not exclusively dominate the heat transfer. Second, the enhancement of the NFRHT due to the external field in this region is due to an increase in the contribution of evanescent TE modes. Very much like in the case studied in the previous section, the enhanced probability of evanescent TE modes upon the application of the field is due to a reduction of the impedance mismatch between InSb and the vacuum gap in frequency regions where the dielectric component ϵ_{xx} exhibits a vanishing real part. For completeness, we also show in Fig 7(c,d) the corresponding spectral heat flux for various field values for the case $t = 2.5 \mu\text{m}$ and $d = 1 \mu\text{m}$. As one can see, the TE spectrum is much more sensitive to the application of an external field than the corresponding TM modes.

V. ANISOTROPIC THERMAL MAGNETORESISTANCE

In Ref. [37] it was predicted that a huge anisotropic thermal magnetoresistance (ATMR) in the near-field radiative heat transfer between MO particles when the direction of an external magnetic field is changed with respect to the heat transport direction. This phenomenon, which is the thermal analog of the famous anisotropic magnetoresistance (AMR) in spintronics [49], was illustrated in the case of two submicron InSb spherical particles. The ATMR was first hinted in our work [33] where we studied the magnetic field dependence of the radiative heat transfer between two identical parallel plates made of doped semiconductors (InSb and Si). There, we noticed the significant difference in the NFRHT between applying the magnetic field perpendicular or parallel to the plates, but we did not analyze systematically the impact of the field direction on the radiative heat conductance. We shall fill this gap in this section by analyzing the NFRHT in the system of Fig. 1(c) where two identical InSb infinite plates are subjected to a magnetic field forming an angle θ_H with the transport direction. In particular, we shall investigate the change in the heat transfer coefficient for a given value of the magnitude of the external field upon changing its orientation relative to the transport direction.

In Fig. 8 we present the results for the dependence of the heat transfer coefficient on the angle θ_H between the external magnetic field and the transport direction, see Fig. 1(c), for different values of the field magnitude and two different values of the gap size in the near-field regime, 10 and 100 nm. In this figure we show the results

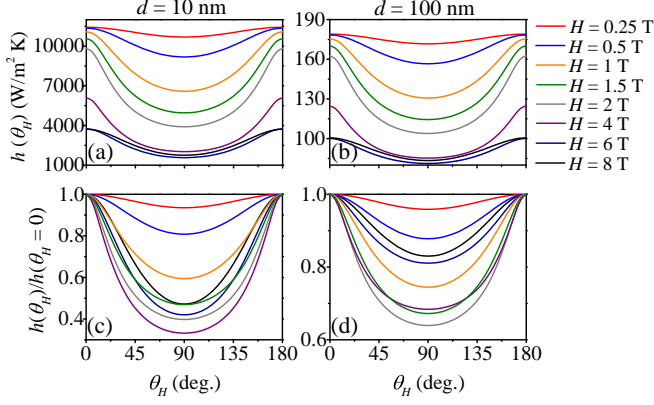


FIG. 8. (a) Heat transfer coefficient for the system of Fig. 1(c) as a function of the angle θ_H between the external field and the transport direction for different values of the magnitude of the magnetic field for a gap size $d = 10 \text{ nm}$. (b) The same as in panel (a), but for $d = 100 \text{ nm}$. (c,d) The same as in panels (a) and (b), respectively, but now the heat transfer coefficient is normalized by its value for $\theta_H = 0$.

for both the absolute value of the heat transfer coefficient, panel (a) and (b), and the ratio between its value at given angle θ_H and its value at $\theta_H = 0$ when the field is perpendicular to the plates, panels (c) and (d). As one can see, the heat transfer coefficient is strongly modulated by the field direction and it is symmetric around $\theta_H = 90^\circ$. In all cases, the conductance is maximum at $\theta_H = 0^\circ$ (when the field is perpendicular to the plates) and it reaches a minimum at $\theta_H = 90^\circ$ (when the field is parallel to the plates). More importantly, the ATMR ratio, defined as $h(\theta_H)/h(\theta_H = 0)$, reaches a minimum, for example, for 1 T of ~ 0.6 for $d = 10 \text{ nm}$ and of ~ 0.75 for $d = 100 \text{ nm}$. In terms of a thermal resistance per unit of area, $R = 1/h$, these ATMR ratios imply relative changes $[R(\theta_H) - R(\theta_H = 0)]/R(\theta_H = 0)$ of approximately 66% and 33%, respectively. These values are indeed remarkable when one compares them with the 1% relative change in the resistance of spintronic devices for similar fields [50]. It is also worth noticing that the heat transfer coefficient is significantly modulated for moderate fields of 0.25 T (see red curves in Fig. 8). Notice also the ATMR ratio does not decrease monotonically with the magnitude of field in the high-field range (above 1 T).

The physical explanation of the angular dependence of the heat transfer coefficient in the near-field regime is quite complex. Some insight can be gained by analyzing the spectral heat flux. We show the results for this quantity in Fig. 9 for a gap of $d = 10 \text{ nm}$ and three different values of the magnitude of the external field (2, 4, and 6 T). The different curves correspond to different value of the angle θ_H and for comparison, we also present the results in the absence of an external field (dashed lines). Notice that the by increasing θ_H from 0° to 90° , the main effect is reduction of the height of the main peaks in the

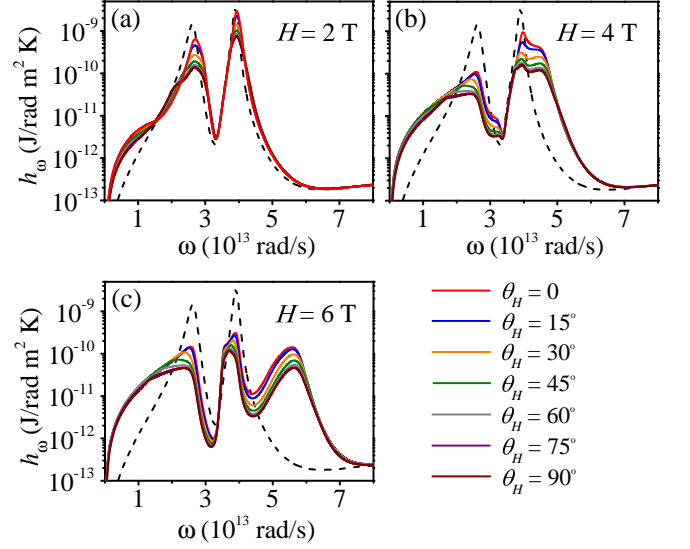


FIG. 9. Spectral heat flux for the system of Fig. 1(c) as a function of the frequency and the angle θ_H between the external field and the transport direction, for a gap of $d = 10 \text{ nm}$. Panels (a), (b) and (c) correspond to a magnetic field magnitude of 2 T, 4 T, and 6 T, respectively. The dashed lines correspond to the zero-field case.

spectra, while the position of those peaks, which are due to the different surface modes present in this system, remains more or less unchanged. A simple interpretation or explanation of these spectra is very difficult due to the fact that for $\theta_H \neq 0$ the radiative heat transfer becomes anisotropic in k -space, see Eq. (2), meaning that it does not longer depend only on the modulus of the parallel wave vector, k , but rather on the exact direction $\mathbf{k} = (k_x, k_y)$. As we showed in Ref. [33], when the field is parallel to the plates, there are a variety of electromagnetic modes that contribute to the NFRHT depending of \mathbf{k} direction. In that particular configuration, surface modes originating from both plasmon and phonon polaritons compete with hyperbolic modes. In particular, the dispersion relation of the surface modes is very sensitive to the external magnetic field, which leads to an even more drastic reduction of the NFRHT than in the case of a field perpendicular to the plates and explains why the heat transfer coefficient reaches a minimum at $\theta_H = 90^\circ$.

VI. CONCLUSIONS

As explained in the introduction, the application of a static magnetic field in combination with MO materials has emerged as a promising way to actively tune and control NFRHT. However, this generic idea has still to be demonstrated experimentally and most of the related thermomagnetic effects predicted in the last few years deal with systems that are extremely challenging

for the experiment. For this reason, we have focused on this work on putting forward a number of novel physical effects related to the NFRHT between planar layered systems containing MO materials that are amenable to measurement with the existent experimental techniques. In particular, we have discussed three basic phenomena. First, we have shown that, contrary to what have been reported so far, it is possible to use a magnetic field to increase the NFRHT. We have demonstrated this possibility with the analysis of an asymmetric system consisting of two parallel plates made of InSb and Au. We have attributed the field-induced enhancement of the NFRHT to the corresponding increase in the contribution of evanescent TE waves due to the reduction of the impedance mismatch between InSb and the vacuum gap in frequency regions where the real part of the InSb refractive index tends to vanish.

The second physical problem that we have explored in this work is the magnetic field dependence of the NFRHT in layered structures of MO materials containing thin films. To be precise, we have studied the radiative heat transfer between an InSb infinite plate and a bilayer structure comprising an InSb thin film deposited on a Au substrate. We have shown that depending on the thickness of the InSb film one can further reduce the NFRHT upon the application of an external field perpendicular to the plate surfaces. We have also found that in the case of films with intermediate thicknesses it is possible to enhance the NFRHT in a certain gap range, contrary to

what happens in bulk counterparts. We have shown that this peculiar effect also originates from the field-induced enhancement of the probability of evanescent TE modes.

Finally, we have analyzed systematically the phenomenon of anisotropic thermal magnetoresistance (ATMR) in the case of two parallel plates made of InSb, extending so our partial analysis of Ref. [33]. We have shown that the NFRHT is very sensitive to the orientation of the external field, with respect to the transport direction, and its modulation only requires moderate magnetic fields. Moreover, the amplitudes of the field modulation of the radiative heat conductance in this simple situation turn out to be orders of magnitude larger than in the case of the electronic analog in the context of spintronic devices.

So, in short, the different phenomena predicted in this work illustrate once more the rich thermal radiation physics that one can encounter when combining an external magnetic field and MO materials. Moreover, they show that the application of an external magnetic field enables to actively control NFRHT in a variety of ways and we are convinced that this work will motivate the realization of experiments to test all these different ideas.

ACKNOWLEDGMENTS

We thank Antonio I. Fernández-Domínguez for fruitful discussions. J.C.C. acknowledges funding from the Spanish Ministry of Economy and Competitiveness (MINECO) (contract No. FIS2017-84057-P).

-
- [1] B. Song, A. Fiorino, E. Meyhofer, and P. Reddy, Near-field radiative thermal transport: From theory to experiment, *AIP Advances* **5**, 053503 (2015).
 - [2] J. C. Cuevas and F. J. García-Vidal, Radiative heat transfer, *ACS Photonics* **5**, 3896 (2018).
 - [3] D. Polder and M. Van Hove, Theory of radiative heat transfer between closely spaced bodies *Phys. Rev. B* **4**, 3303 (1971).
 - [4] S. M. Rytov, *Theory of Electric Fluctuations and Thermal Radiation*, (Air Force Cambridge Research Center, Bedford, MA, 1953).
 - [5] S. M. Rytov, Y. A. Kravtsov, and V. I. Tatarskii, *Principles of Statistical Radiophysics*, Vol. 3 (Springer-Verlag, Berlin Heidelberg, 1989).
 - [6] C. M. Hargreaves, Anomalous radiative transfer between closely-spaced bodies, *Phys. Lett. A* **30**, 491 (1969).
 - [7] G. A. Domoto, R. F. Boehm, and C. L. Tien, Experimental investigation of radiative transfer between metallic surfaces at cryogenic temperatures, *J. Heat Transfer* **92**, 412 (1970).
 - [8] A. Kittel, W. Müller-Hirsch, J. Parisi, S.-A. Biehs, D. Reddig, and M. Holthaus, Near-field heat transfer in a scanning thermal microscope, *Phys. Rev. Lett.* **95**, 224301 (2005).
 - [9] A. Narayanaswamy, S. Shen, and G. Chen, Near-field radiative heat transfer between a sphere and a substrate, *Phys. Rev. B* **78**, 115303 (2008).
 - [10] L. Hu, A. Narayanaswamy, X. Y. Chen, and G. Chen, Near-field thermal radiation between two closely spaced glass plates exceeding Plancks blackbody radiation law, *Appl. Phys. Lett.* **92**, 133106 (2008).
 - [11] E. Rousseau, A. Siria, G. Jourdan, S. Volz, F. Comin, J. Chevrier, and J.-J. Greffet, Radiative heat transfer at the nanoscale, *Nat. Photonics* **3**, 514 (2009).
 - [12] S. Shen, A. Narayanaswamy, and G. Chen, Surface phonon polaritons mediated energy transfer between nanoscale gaps, *Nano Lett.* **9**, 2909 (2009).
 - [13] R. S. Ottens, V. Quetschke, S. Wise, A. A. Alemi, R. Lundock, G. Mueller, D. H. Reitze, D. B. Tanner, and B. F. Whiting, Near-field radiative heat transfer between macroscopic planar surfaces, *Phys. Rev. Lett.* **107**, 014301 (2011).
 - [14] S. Shen, A. Mavrokefalos, P. Sambegoro, and G. Chen, Nanoscale thermal radiation between two gold surfaces, *Appl. Phys. Lett.* **100**, 233114 (2012).
 - [15] T. Kralik, P. Hanzelka, M. Zobac, V. Musilova, T. Fort, and M. Horak, Strong near-field enhancement of radiative heat transfer between metallic surfaces, *Phys. Rev. Lett.* **109**, 224302 (2012).
 - [16] P. J. van Zwol, L. Ranno, and J. Chevrier, Tuning near field radiative heat flux through surface excitations with a metal insulator transition, *Phys. Rev. Lett.* **108**, 234301

- (2012).
- [17] P. J. van Zwol, S. Thiele, C. Berger, W. A. de Heer, and J. Chevrier, Nanoscale radiative heat flow due to surface plasmons in graphene and doped silicon, *Phys. Rev. Lett.* **109**, 264301 (2012).
 - [18] B. Guha, C. Otey, C. B. Poitras, S. H. Fan, and M. Lipson, Near-field radiative cooling of nanostructures, *Nano Lett.* **12**, 4546 (2012).
 - [19] J. Shi, P. Li, B. Liu, and S. Shen, Tuning near field radiation by doped silicon, *Appl. Phys. Lett.* **102**, 183114 (2013).
 - [20] L. Worbes, D. Hellmann, and A. Kittel, Enhanced near-field heat flow of a monolayer dielectric island, *Phys. Rev. Lett.* **110**, 134302 (2013).
 - [21] R. St-Gelais, B. Guha, L. X. Zhu, S. H. Fan, and M. Lipson, Demonstration of strong near-field radiative heat transfer between integrated nanostructures, *Nano Lett.* **14**, 6971 (2014).
 - [22] B. Song, Y. Ganjeh, S. Sadat, D. Thompson, A. Fiorino, V. Fernández-Hurtado, J. Feist, F. J. Garcia-Vidal, J. C. Cuevas, P. Reddy, and E. Meyhofer, Enhancement of near-field radiative heat transfer using polar dielectric thin films, *Nat. Nanotechnol.* **10**, 253 (2015).
 - [23] K. Kim, B. Song, V. Fernández-Hurtado, W. Lee, W. Jeong, L. Cui, D. Thompson, J. Feist, M. T. H. Reid, F. J. García-Vidal, J. C. Cuevas, E. Meyhofer, P. Reddy, Radiative heat transfer in the extreme near field, *Nature (London)* **528**, 387 (2015).
 - [24] M. Lim, S. S. Lee, and B. J. Lee, Near-field thermal radiation between doped silicon plates at nanoscale gaps, *Phys. Rev. B* **91**, 195136 (2015).
 - [25] R. St-Gelais, L. Zhu, S. Fan, and M. Lipson, Near-field radiative heat transfer between parallel structures in the deep subwavelength regime, *Nat. Nanotechnol.* **11**, 515 (2016).
 - [26] B. Song, D. Thompson, A. Fiorino, Y. Ganjeh, P. Reddy, E. Meyhofer, Radiative heat conductances between dielectric and metallic parallel plates with nanoscale gaps, *Nat. Nanotechnol.* **11**, 509 (2016).
 - [27] M. P. Bernardi, D. Milovich, M. Francoeur, Radiative heat transfer exceeding the blackbody limit between macroscale planar surfaces separated by a nanosize vacuum gap, *Nat. Comm.* **7**, 12900 (2016).
 - [28] L. Cui, W. Jeong, V. Fernández-Hurtado, J. Feist, F. J. García-Vidal, J. C. Cuevas, E. Meyhofer, P. Reddy, Study of radiative heat transfer in Ångström- and nanometre-sized gaps, *Nat. Commun.* **8**, 14479 (2017).
 - [29] K. Klopstech, N. Köne, S.-A. Biehs, A. W. Rodriguez, L. Worbes, D. Hellmann, A. Kittel, Giant heat transfer in the crossover regime between conduction and radiation, *Nat. Commun.* **8**, 14475 (2018).
 - [30] M. Ghashami, H. Geng, T. Kim, N. Iacopino, S.-K. Cho, K. Park, Precision measurement of phonon-polaritonic near-field energy transfer between macroscale planar structures under large thermal gradients, *Phys. Rev. Lett.* **120**, 175901 (2018).
 - [31] A. Fiorino, D. Thompson, L. Zhu, B. Song, P. Reddy, E. Meyhofer, Giant enhancement in radiative heat transfer in sub-30 nm gaps of plane parallel surfaces, *Nano Lett.* **18**, 3711 (2018).
 - [32] J. DeSutter, L. Tang, and M. Francoeur, A near-field radiative heat transfer device, *Nat. Nanotechnol.* **14**, 751 (2019).
 - [33] E. Moncada-Villa, V. Fernández-Hurtado, F. J. García-Vidal, A. García-Martín, and J. C. Cuevas, Magnetic field control of near-field radiative heat transfer and the realization of highly tunable hyperbolic thermal emitters, *Phys. Rev. B* **92**, 125418 (2015).
 - [34] P. Ben-Abdallah, Photon thermal Hall effect, *Phys. Rev. Lett.* **116**, 084301 (2016).
 - [35] L. Zhu and S. Fan, Persistent directional current at equilibrium in nonreciprocal many-body near field electromagnetic heat transfer, *Phys. Rev. Lett.* **117**, 134303 (2016).
 - [36] I. Latella and P. Ben-Abdallah, Giant thermal magnetoresistance in plasmonic structures, *Phys. Rev. Lett.* **118**, 173902 (2017).
 - [37] R. M. Abraham Ekeröth, P. Ben-Abdallah, J. C. Cuevas, and García-Martín, Anisotropic thermal magnetoresistance for an active control of radiative heat transfer, *ACS Photonics* **5**, 705 (2018).
 - [38] A. Ott, R. Messina, P. Ben-Abdallah, and S.-A. Biehs, Magnetothermoplasmonics: from theory to applications, *J. Photon. Energy* **9**, 032711 (2019).
 - [39] E. Moncada-Villa, A. I. Fernández-Domínguez, J. C. Cuevas, Magnetic-field controlled anomalous refraction in doped semiconductors, *J. Opt. Soc. Am. B* **36**, 935 (2019).
 - [40] A. Poddubny, I. Iorsh, P. Belov, and Y. Kivshar, Hyperbolic metamaterials, *Nat. Photonics* **7**, 948 (2013).
 - [41] A. Zvezdin and V. Kotov, *Modern Magneto-optics and Magneto-optical Materials*, (IOP, Bristol, 1997).
 - [42] S.-A. Biehs, P. Ben-Abdallah, F. S.S. Rosa, K. Joulain, and J.-J. Greffet, Nanoscale heat flux between nanoporous materials, *Opt. Express* **19**, A1088 (2011).
 - [43] B. Caballero, A. García-Martín, and J. C. Cuevas, Generalized scattering-matrix approach for magneto-optics in periodically patterned multilayer systems, *Phys. Rev. B* **85**, 245103 (2012).
 - [44] E. D. Palik, R. Kaplan, R. W. Gammon, H. Kaplan, R. F. Wallis, and J. J. Quinn, Coupled surface magnetoplasmon-optic-phonon polariton modes on InSb, *Phys. Rev. B* **13**, 2497 (1976).
 - [45] P. O. Chapuis, S. Volz, C. Henkel, K. Joulain, and J. J. Greffet, Effects of spatial dispersion in near-field radiative heat transfer between two parallel metallic surfaces, *Phys. Rev. B* **77**, 035431 (2008).
 - [46] S.-A. Biehs, Thermal heat radiation, near-field energy density and near-field radiative heat transfer of coated materials, *Eur. Phys. J. B* **58**, 423 (2007).
 - [47] S. Basu and Z. M. Zhang, Ultrasmall penetration depth in nanoscale thermal radiation, *Appl. Phys. Lett.* **95**, 133104 (2009).
 - [48] M. Francoeur, M. P. Menguc, and R. Vaillon, Coexistence of multiple regimes for near-field thermal radiation between two layers supporting surface phonon polaritons in the infrared, *Phys. Rev. B* **84**, 075436 (2011).
 - [49] I. Žutić, J. Fabian, and S. Das Sarma, Spintronics: Fundamentals and applications, *Rev. Mod. Phys.* **76**, 323 (2004).
 - [50] R. C. O'Handley, *Modern Magnetic Materials: Principles and Applications*, (Wiley, 2000).